Theoretical Computations of the Effects of the Metastable Populations on Electron Energy Balance and Distribution Function in a Helium Afterglow

W. E. Wells, P. Monchicourt, R. Deloche, and J. Berlande
Service de Physique Atomique, Centre d'Etudes Nucléaires de Saclay, 91 Gif-sur-Yvette, France
(Received 22 November 1972)

The electron temperatures and the electron energy distribution function in a helium afterglow, for pressures of 10–80 Torr and electron densities of 10^{11}–10^{13} cm^{-3}, are calculated by a technique which readily allows the determination of the relaxation processes controlling the energy input into the electron gas. Comparisons are made to existing experimental data. The energy-distribution-function evaluations show that careful consideration of this parameter must be made, for it can be extremely non-Maxwellian.

I. INTRODUCTION

Recently, experimental evidence in a helium afterglow at 300 °K[1] of an elevated electron temperature in a pressure range from 10 to 80 Torr and for electron densities from 5×10^{10} to 7×10^{11} cm^{-3}, has been presented.

Many investigators have previously assumed that, under these experimental conditions, the electron temperature is equal to the gas temperature. The experimental results[1] have prompted a theoretical analysis of the electron energy balance and electron distribution function in the helium afterglow. Two other measurements also indicate elevated electron temperatures. At 10 Torr, Miller *et al.*[2] deduced the electron temperature from the evaluation of average electron-neutral collision frequency measurements. At 44.6 Torr, Collins *et al.*[3] using optical spectrometry, evaluated the electron temperature from precise measurements of the continuum radiation. This characteristic of an elevated electron temperature in the helium afterglow is supported by the variety of diagnostic methods used in its determination. Delpech[4] has also reported the observation of an elevated electron temperature, measured with a transmission-type microwave radiometer, at 20 Torr.

Because of the very energetic electrons produced by some of the basic processes in the helium afterglow (Sec. II), it is necessary to examine the interaction of these "hot" electrons with the background electrons and neutrals. In this examination we show the partition of energy between the background electrons and neutrals (Sec. III). Also in Sec. III we show the influence of the relaxation of these "hot" electrons on the Maxwellian energy distribution function. These two calculations form the major contribution of this paper. Standard analyses[2,5–7] have been used for the evaluation of the quasi-steady-state electron temperature (Sec. IV). The temperatures calculated are compared to experiment in Sec. V. The effects of the non-Maxwellian electron energy distribution function for the case of the electron radiation temperature are presented in Sec. VI.

II. BASIC PROCESSES INFLUENCING THE ELECTRON ENERGY EVOLUTION DURING THE AFTERGLOW

During the afterglow, a quasi-steady-state temperature is reached when the processes which tend to heat the electron distribution balance the processes which tend to cool it. For this reason we have divided the basic processes into these two groups for this discussion.

The major heating processes have been found to involve the metastable states. Very energetic electrons[8] are released by metastable-metastable interactions,

$$\mathrm{He}(2\,^3S)+\mathrm{He}(2\,^3S)\rightarrow \mathrm{He}^+ + \mathrm{He} + e \quad (15\ \mathrm{eV}), \tag{1}$$

$$\mathrm{He}(2\,^1S)+\mathrm{He}(2\,^1S)\rightarrow \mathrm{He}^+ + \mathrm{He} + e \quad (16.6\ \mathrm{eV}), \tag{2}$$

$$\mathrm{He}_2(2\,^3\Sigma)+\mathrm{He}_2(2\,^3\Sigma)\rightarrow \mathrm{He}^+ + 3\mathrm{He} + e \quad (11.3\ \mathrm{eV}) \tag{3a}$$

$$\rightarrow \mathrm{He}_2^+ + 2\mathrm{He} + e \quad (13.7\ \mathrm{eV}). \tag{3b}$$

The rate constants for these processes and for the other processes which are described in this section are presented in Table I. The relative importance of the above reactions depends on the relative populations of the three metastable states. It should also be pointed out that collisions between different metastable states are possible but that the rate constants for these are unknown.

Another source of electron energy comes from electron-metastable collisions:

$$\mathrm{He}(2\,^3S)+e\rightarrow \mathrm{He}+e \quad (19.8\ \mathrm{eV}), \tag{4}$$

TABLE I. Rate constants for the processes discussed in the text, together with the references for their sources.

Process	Rate constant	References
(1)	$\beta = 1.8\times10^{-9}$ cm^3 sec^{-1}	Phelps and Molnar (Ref. 9).
(2)	$\beta = 1.8\times10^{-9}$ cm^3 sec^{-1}	Assumed to be equal to the rate of process (1).
(3)	$\beta = 4\times10^{-9}$ cm^3 sec^{-1}	Phelps (Ref. 13).
(4)	$\gamma = 7\times10^{-11}\, T_e^{1/2}$ cm^3 sec^{-1} for $T_e < 2000$ °K	Deduced by detailed balancing from the work of Schultz and Fox (Ref. 10).
(5)	$\gamma = 7\times10^{-11}\, T_e^{1/2}$ cm^3 sec^{-1}	Assumed to be equal to the rate of process (4).
(6)	$\gamma = 7\times10^{-11}\, T_e^{1/2}$ cm^3 sec^{-1}	Assumed to be equal to the rate of process (4).
(7)	$\delta = 3.5\times10^{-7}$ cm^3 sec^{-1}	Phelps (Ref. 13).
(8) and (9)	$k_{e0} = \begin{cases} 3.7\times10^{-8}\,\epsilon^{1/2} \text{ cm}^3\text{ sec}^{-1} & \text{for } \epsilon \le 3 \text{ eV} \\ 6.5\times10^{-8} \text{ cm}^3\text{ sec}^{-1} & \text{for } \epsilon \ge 3 \text{ eV} \end{cases}$	Analytical approximation of the values of Brown (Ref. 14).
(10)	$k_{ee} = 7.7\times10^{-6}\epsilon^{-3/2}\ln\Lambda$ for $\epsilon > \frac{3}{2}kT_e$ with $\ln\Lambda = \ln[5\times10^9\epsilon(kT_e/n_e)^{1/2}]$ (ϵ in eV)	Delcroix (Ref. 11). Spitzer (Ref. 12).

$$\mathrm{He}(2\,^1S) + e \rightarrow \mathrm{He} + e \quad (20.6\ \mathrm{eV}), \tag{5}$$

$$\mathrm{He}_2(2\,^3\Sigma) + e \rightarrow 2\mathrm{He} + e \quad (17.9\ \mathrm{eV}), \tag{6}$$

and

$$\mathrm{He}(2\,^1S) + e \rightarrow \mathrm{He}(2\,^3S) + e \quad (0.79\ \mathrm{eV}). \tag{7}$$

The last process (7) does not form a significant heating process, but because of the large rate constant (Table I) depletes the $2\,^1S$ population very efficiently. During the afterglow the processes involving the He($2\,^1S$) can be ignored.

Another heating process considered was electron-ion recombination. Computations utilizing the experimental analysis of Berlande et al.[15] indicated the heating due to this process is negligible in comparison with the processes involving the metastables.

The processes which tend to cool the electron energy distribution are better known and easier to identify than the heating processes. In this investigation the major cooling process was electron-neutral collisions,

$$e(\epsilon_1) + \mathrm{He}(\epsilon_2) \rightarrow e(\epsilon_1 - \Delta\epsilon) + \mathrm{He}(\epsilon_2 + \Delta\epsilon), \tag{8}$$

where the average energy transferred in this collision is

$$\langle\Delta\epsilon\rangle = (2m/M_{\mathrm{He}})(\langle\epsilon_1\rangle - \langle\epsilon_2\rangle). \tag{9}$$

Other cooling processes which have been investigated but found to be negligible are electron-ion collisions, diffusion of electrons, and thermal conduction. The latter two depend on the spatial distribution of the electron density; their importance as cooling processes depend on experimental conditions, e.g., cell size and pressure. In experiment[1] these two quantities were negligible.

Processes (1)–(7) each produce electrons which are too energetic to be considered part of the background-electron gas. As has been pointed out by Miller *et al.*[2] and Mosburg,[7] these hot electrons are thermalized by electron-neutral collisions (8) and electron-electron collisions,

$$e(\epsilon_1) + e(\epsilon_2) \rightarrow e(\epsilon_1 - \Delta\epsilon) + e(\epsilon_2 + \Delta\epsilon). \tag{10}$$

Each of these processes is well known individually (Table I), but their simultaneous actions must be considered very carefully, because they produce a partition of energy between the background electrons and neutrals. In addition, the continuous relaxation of these hot electrons results in a residual population of energetic electrons, which creates a perturbation to the energy distribution function of the background electrons. These points are considered in detail in Sec. III.

III. RELAXATION OF NON-MAXWELLIAN ELECTRONS TO A MAXWELLIAN DISTRIBUTION

The non-Maxwellian electrons relax in collisions with Maxwellian electrons (10) and neutrals (8).

Although the interaction of the non-Maxwellian electron with the background electrons is typically calculated on the basis of binary discrete collisions, in reality it undergoes a continuous loss process because of its long-range interaction with the other electrons, and consequently interacts with all of the electrons within its Debye sphere. The electron-neutral interaction is a binary process, which produces discrete changes in the electron energy.

Within this framework, the calculation of the energy transferred to the background-electron gas is a simple accumulation of the amount of energy lost to the Maxwellian electrons between collisions with neutrals. The scheme of this calculation is shown in Fig. 1. A non-Maxwellian electron is produced at some energy ϵ_0 by one of the binary collision processes described above. It undergoes a continuous loss by interactions with Maxwellian electrons until interrupted at a time $1/\nu_{e0}$ by a collision with a neutral. At this statistical time there is an abrupt loss of energy by this binary collision. After this interruption, its electron-electron loss process continues until the next electron-neutral collision. The energy transferred to the Maxwellian electrons is then

$$\Delta\epsilon'_{ee} = \sum_{n=0}^{n_c} (\Delta\epsilon_{ee})_n, \tag{11}$$

where $(\Delta\epsilon_{ee})_n$ is the energy lost to the Maxwellian electrons between the $(n-1)$th and nth collision with neutrals, and n_c is the total number of collisions required in order to provide for the relaxation of the non-Maxwellian electron. The energy transferred to the neutrals is then

$$\Delta\epsilon'_{en} = \epsilon_0 - \Delta\epsilon'_{ee}. \tag{12}$$

The results of the calculation are shown in Fig. 2 for a Maxwellian background distribution of electrons at 300 °K. In this figure, the parameter of variation is the ratio of the electron density to the pressure of the neutral gas P. It is interesting to note that for low values of this ratio, the energy transferred to the Maxwellian electrons is almost independent of the initial energy of the non-Maxwellian electron. For the energy balance when the N_e/P ratio is below 1×10^{11}, it does not matter which metastable is considered or which of the processes previously described produces the non-Maxwellian electron—it will transfer approximately the same amount of energy to the Maxwellian electrons. Thus, for the calculation of the energy balance, it is the total density of metastables which is important. For comparison, the energy transferred to the Maxwellian electrons as calculated by Miller *et al.*[2] using an approximate formula is also plotted in Fig. 2 for N_e/P equal to 10^{10} and 10^{11} cm^{-3} Torr^{-1} (dashed lines).

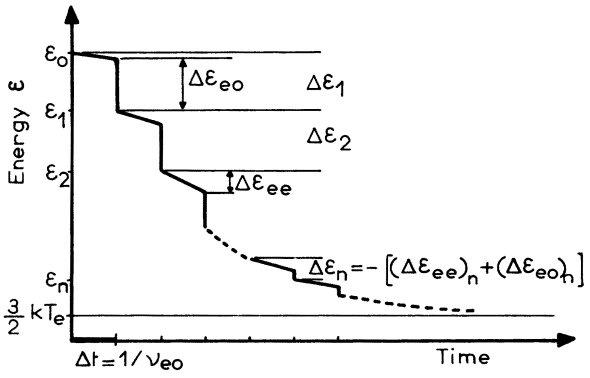

FIG. 1. Calculation scheme for the relaxation of a non-Maxwellian electron by collisions with Maxwellian electrons and background neutrals.

It is desirable at this point to investigate the assumption of a Maxwellian electron distribution. From the calculation scheme described above, the relaxation time τ for a non-Maxwellian electron can be calculated by

$$\tau = \sum_{n=0}^{n_c} 1/(\nu_{e0})_n. \tag{13}$$

Examples of this relaxation time are shown in Fig. 3 for several conditions of electron densities and pressures. The results of this calculation on an incremental basis allow the calculation of the electron energy distribution function. With this incremental relaxation time and the concept of

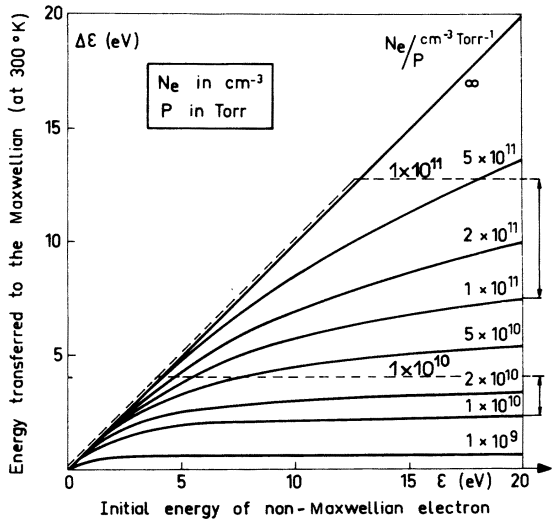

FIG. 2. Heating of a Maxwellian electron distribution by the relaxation of a non-Maxwellian electron of initial energy ϵ_0. For comparison, the energy transferred to the Maxwellian electrons at 300 °K calculated by Ref. 2 are given for $N_e/P = 10^{11}$ and 10^{10} cm^{-3} Torr^{-1} (dashed lines).

particle conservation in the flux into and out of an incremental energy slice, the following relationship was used to calculate the steady-state population of electrons within an incremental energy slice,

$$n_i = \tau_i[n_{i-1}/\tau_{i-1} + \tfrac{1}{2}\beta M^2 \delta(\epsilon_i - 15) + \gamma M N_e \delta(\epsilon_i - 19.8)], \quad (14)$$

where n_i is the population of the energy increment, and τ_{i-1} is the relaxation time from increment $i-1$ to i. The first term within the square brackets on the right-hand side of Eq. (14) represents the flux of electrons which have relaxed from the preceding energy slice. The second term is the flux of electrons from atomic metastable-metastable ionization (1) at 15 eV with a Dirac δ-function distribution of initial energy. The third term is again a Dirac δ function representing the flux of electrons at 19.8 eV owing to the superelastic relaxation of the atomic metastable (4). The solution of Eq. (14) yields the electron population in each incremental energy slice, which acts as a perturbation to the Maxwellian distribution. Figure 4 shows three examples of this perturbation. Also included in this figure is the Maxwellian distribution for comparison. For this calculation, the metastable density was assumed to be equal to the electron density.

In this figure the total electron energy distribution function is given by

$$f = f_{\text{Max}} + \Delta f, \quad (15)$$

where f is the electron energy distribution function, f_{Max} is a Maxwellian distribution, and Δf is the perturbation due to the relaxation of hot electrons. In the cases illustrated here, the Maxwellian-electron temperature and the neutral-gas temperature are both set equal to 300 °K. At a pressure of 10 Torr and electron density of 10^{12} cm^{-3}, approximately 10% of the energy and 0.1% of the population are contained in the perturbation term. Only one metastable species is represented in the perturbation part of the distribution. If all of the metastable species were represented in the theory, there would be four more injection points visible in Fig. 4. Since process (7) provides for a very efficient depletion of the He(2 ^{1}S) by conversion to He(2 ^{3}S), it is reasonable to neglect this population. However, very little information is available on the relative concentrations of the He(2 ^{3}S) and He(2 $^3\Sigma$). The approximation that the total metastable population can be represented by a single metastable with the characteristics of the He(2 ^{3}S) makes no error for the distribution below 11.3 eV, but the overestimation in total population which would result, if the molecular metastable were the dominant metastable in the afterglow, would be approximately 20%.

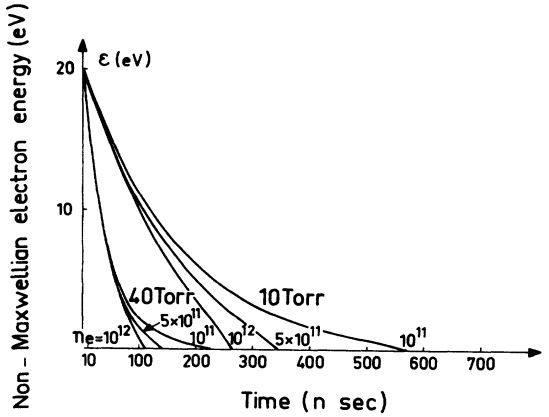

FIG. 3. Relaxation time for a 20-eV electron for two pressures of 10 and 40 Torr and three electron densities 10^{11}, 5×10^{11}, and 10^{12} cm^{-3}.

It should be emphasized that all of the metastables could easily be accomodated in this type of calculation if the relative populations were known.

The partition of the energy of non-Maxwellian electrons and the total energy distribution function can be very well approximated by analytical calculations as is shown in the Appendix.

IV. CALCULATION MODEL FOR THE QUASI-STEADY-STATE TEMPERATURE

As has been shown in Sec. III, under the conditions described here, the heating due to the metastable population is insensitive to the species of metastable. For this reason a simplification can be made in the calculations of this section,

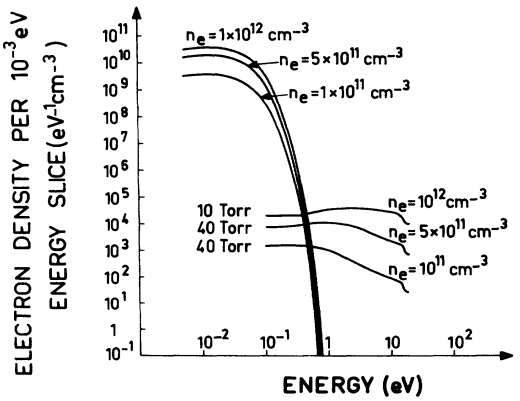

FIG. 4. Three examples of the electron energy distribution function. The incremental energy size for this calculation was 10^{-3} eV. For each of the curves, the metastable density is assumed equal to the electron density, and the electron temperature of the Maxwellian part in 300 °K. The total distribution function, for each experimental condition, is the sum of the Maxwellian part and the perturbation.

which conserves only one metastable, the He(2^3S), to represent the total metastable population. With this simplification, heating processes to be considered are Eqs. (1) and (4); the cooling is due to Eq. (8). The other processes are either negligible or not appropriate to the one-metastable approximation.

The energy balance is formed by

$$\frac{\delta}{\delta t}\left(\tfrac{3}{2}kT_eN_e\right) = -\frac{3m}{M_{\mathrm{He}}}k_{e0}N_0k(T_e-T_0)N_e \quad \text{(electron-neutral collisions)}$$
$$+\tfrac{1}{2}\beta M^2\Delta\epsilon'_{\mathrm{mm}} \quad \text{(metastable-metastable collisions)}$$
$$+\gamma MN_e\Delta\epsilon'_{\mathrm{se}} \quad \text{(superelastic relaxation)}, \tag{16}$$

where k is the Boltzmann constant, T_e is the electron temperature, N_e is the electron density, M_{He} is the mass of the atom, and m is the mass of the electron; the rate constants k_{e0}, β, and γ are defined in Table I.

With the knowledge of the energy transferred to the electron gas and the validity of the assumption of the Maxwellian distribution from Sec. III, the energy balance can be evaluated. The left-hand side of Eq. (16) can be written as

$$\frac{\delta}{\delta t}\left(\tfrac{3}{2}kN_eT_e\right) = \tfrac{3}{2}kN_e\frac{\delta T_e}{\delta t} + \tfrac{3}{2}kT_e\frac{\delta N_e}{\delta t}. \tag{17}$$

The second term of the expansion represents the change in the total energy of the distribution by electrons gained or lost at the mean energy of the distribution. This term is small compared to the terms on the right-hand side of (17), and can be ignored. The quasi-steady-state assumption requires

$$(3m/M_{\mathrm{He}})k_{e0}N_0k(T_e-T_0)N_e = \tfrac{1}{2}\beta M^2\Delta\epsilon'_{\mathrm{mm}} + \gamma MN_e\Delta\epsilon'_{\mathrm{se}}. \tag{18}$$

The values which satisfy this equation are shown in Fig. 5 for three sample pressures of 10, 40, and 80 Torr. In this figure, the variation of electron temperature is shown as a function of electron density for constant metastable densities. At the low pressure of 10 Torr, the temperature can increase with increasing electron density, even though the metastable density remains constant because of the electron-density dependence of the partition of energy (Fig. 2).

Figure 6 illustrates the variation of the electron temperature with pressure over the range 10–80 Torr, for constant electron and metastable densities. Two values of the total metastable density are chosen for each electron density.

V. COMPARISON OF THEORY TO EXPERIMENT

Some of the experimental evidence of the elevated electron temperature in the helium afterglow, discussed in the Introduction, is shown in Fig. 7. Here the data from the experimental work of the

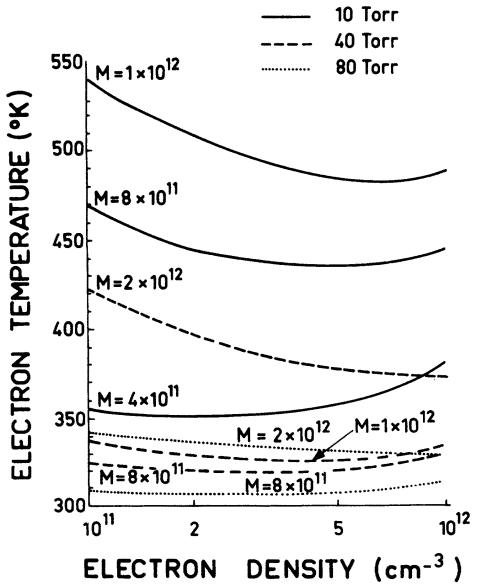

FIG. 5. Theoretical electron temperature vs electron density at constant metastable densities, for different pressures.

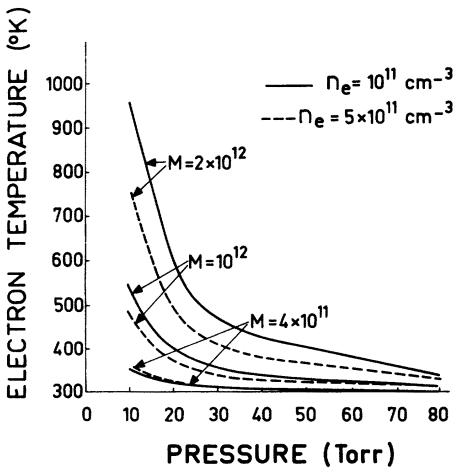

FIG. 6. Electron temperature vs pressure for several values of electron and metastable densities.

authors[1] have been compiled at 10, 20, 40, and 80 Torr. In this figure the temperatures measured are shown to be well elevated above the temperature of the gas at 300 °K.

For comparison of experimental results such as these to the calculations presented here, the total density of metastables must be known, as well as the electron temperature in a differential region. The temperatures shown in Fig. 7 are average values weighted over the cross-sectional area of the cell.

It is beneficial at this point to examine some of the implications of the calculations on experiments such as those described in Ref. 1. It can be shown by the calculation of temperatures in adjacent differential regions progressing across the radius of the cell, that the thermal conductivity between these regions is insufficient to perturb a spacial temperature distribution of Bessel-function form if the metastable and electron densities also have Bessel-function distributions. This indicates that the spacial temperature distribution will not be uniform as is often assumed.

Because the electron-temperature distribution is nonuniform, the measurements of temperature[1,2,4] represent weighted average values. This weighting is toward the maximum values in the center of the cells and is dependent on the spacial distributions of electron density and temperature. Thus, accurate comparisons of these calculations and experiments cannot be made without knowledge of these spacial distributions.

Only in the case of the experiment of Miller *et al.*[2] were the densities of the He($2\,^3S$) also reported. By using these densities and the results of the partition of energy in this work, we have calculated the quasi-steady-state temperatures, on the axis of the cell, which correspond to the conditions of their experiment at 10 Torr. These are presented in Fig. 8 (dashed line) along with a replot of their experimental data (large dots). The experimental data must be considered to be lower limit to the temperature on the axis of the cell, for the reasons given above. How closely they represent this temperature depends on the spacial distribution. The dotted line in this figure represents the calculated temperatures of Ref. 2. Their calculations overestimated the energy transferred by the hot electrons to the background-electron gas (see Fig. 2), which in turn overestimates the electron temperature for each differential volume of the plasma. Moreover, they assumed the temperature to have a uniform distribution with parabolic spacial distributions for the electron and metastable densities. The last curve presented in this figure (alternating line) is our effort to take the spacial distributions into account. For this, we have assumed parabolic distributions of electron density and temperature. No quantitative conclusions can be drawn from this curve because

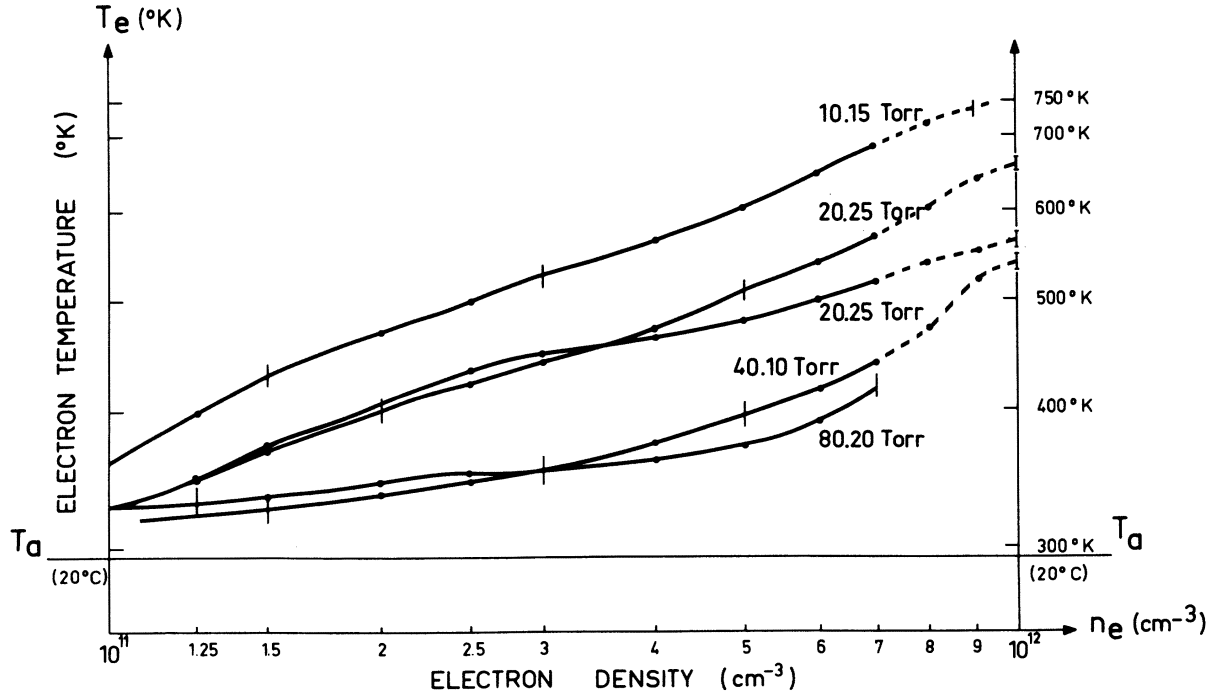

FIG. 7. Experimental evidences of the elevated electron temperature at 10, 20, 40, and 80 Torr. Experimental results obtained by the authors (Ref. 1) using a reflection-type X-band radiometer.

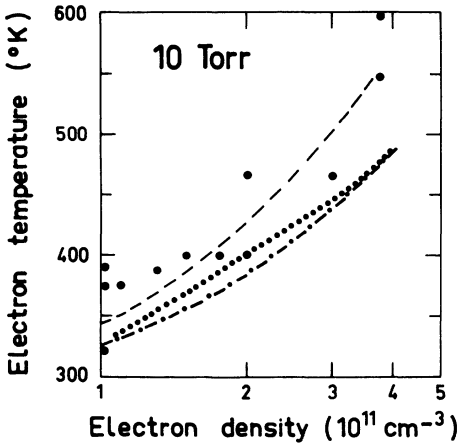

FIG. 8. Comparison of theoretical electron temperatures to experimentally measured values at a pressure of 10 Torr. The experimental and theoretical results of Miller, Verdeyen, and Cherrington (Ref. 2) are represented by large dots and small dots, respectively. The computed curve obtained with our theoretical model, using the metastable and electron densities of Miller *et al.* on the axis of the cell is represented by a dashed line. The weighted average temperature obtained from the curve above (dashed line) and assumed parabolic distributions of electron density and temperature is represented by a line of alternate dashes and dots.

of the sensitive nature of the weighted average temperature on the assumed distributions; the results are presented only to indicate that the theory predicts temperatures somewhat lower than the measured values. This discrepancy could be due to the importance of the helium molecular metastable. At this pressure and above, the molecular ion is dominant and one could also expect the molecular metastable to play a role in the electron energy balance, but for the experiment[2] this quantity was not measured.

More experimental data on electron temperature along with the electron and metastable densities [$He(2^3S)$, $He_2(2\,^3\Sigma)$] and their distributions are needed to confirm the dominance of the metastables as the primary cause of the elevated electron temperature in the afterglow.

VI. EFFECTS OF THE NON-MAXWELLIAN PART OF THE ELECTRON ENERGY DISTRIBUTION FUNCTION

The effect of the perturbation to the Maxwellian distribution function discussed in Sec. III can only be examined in terms of the energy dependence of the quantity being considered. The results the authors displayed in Fig. 7 utilized a microwave radiometer to measure the radiation temperature. This quantity is therefore a good example to examine in terms of the distribution function. With the knowledge of the distribution function calculated in Sec. III, the radiation temperature was evaluated by[16]

$$kT_r = -\int_0^\infty \frac{\nu_{e0}}{\nu_{e0}^2+\omega^2} v^4 f(v)\, dv \Big/ \int_0^\infty \frac{\nu_{e0}}{\nu_{e0}^2+\omega^2} v^4 \frac{1}{mv}\frac{\partial f(v)}{\partial v}\, dv, \tag{19}$$

where k is the Boltzmann constant, T_r is the radiation temperature, m is the mass of the electron, v is the velocity of the electron, $f(v)$ is the distribution function, ν_{e0} is the collision frequency, and ω is the frequency of radiation. For this calculation, the value of ω was taken to be the center frequency of the experiment, 9375 MHz.

Figure 9 indicates the deviation D from the Maxwellian as a function of electron density for two examples of the ratio of metastable-to-electron density for each pressure. The deviation D is calculated as

$$D = (T_r - T_e)/T_e, \tag{20}$$

where T_r is the radiation temperature of the electrons and T_e is the equivalent electron temperature of the Maxwellian part of the distribution function. The value of this temperature was taken in each case as the quasi-steady-state temperature determined by the energy balance described in Sec. IV. In this example, at 10 Torr and for metastable-to-electron density ratio of 4, a deviation of up to 15% from the equivalent temperature of the Maxwellian part can be expected by the measurement of the radiation temperature. At higher pressures the deviation is much less sensitive.

A similar analysis for the collision-frequency determination of the electron temperature, based on the absorption of the afterglow shows a very small sensitivity to perturbations to the Maxwellian distribution of the type shown in Fig. 4.

VII. CONCLUSIONS

Accurate calculations of the partition of energy between Maxwellian electrons and the background neutral gas have been made for the relaxation of very energetic non-Maxwellian electrons produced by reactions such as (1) and (4). The basic calculation has allowed the evaluation of the electron energy balance and the energy distribution function. This evaluation was carried out for the range of electron densities 10^{11}–10^{13} cm^{-3} and over the pressure range 10–80 Torr. The quasi-

steady-state equilibrium temperatures which resulted from the energy balance were compared to existing experimental data.

The model used for the above calculations assumed only one metastable with the characteristics of the $He(2\,^3S)$ metastable. The characteristics of the partition of energy makes this a good approximation for the electron energy balance. The energy distribution function has stronger dependence on the species of metastables, but if the dominant metastable were the molecular metastable, $He_2(2\,^3\Sigma)$ instead of the atomic metastable, then there would be approximately a 20% overestimation of the perturbation density in the calculations.

The effect of the perturbation to the electron energy distribution must be examined in terms of the energy dependence of the quantity being considered. As an example, we have chosen the radiation temperature. The results of this calculation show that extreme care must be taken in applying the assumptions of a Maxwellian distribution, and each quantity must be examined in terms of its energy dependence.

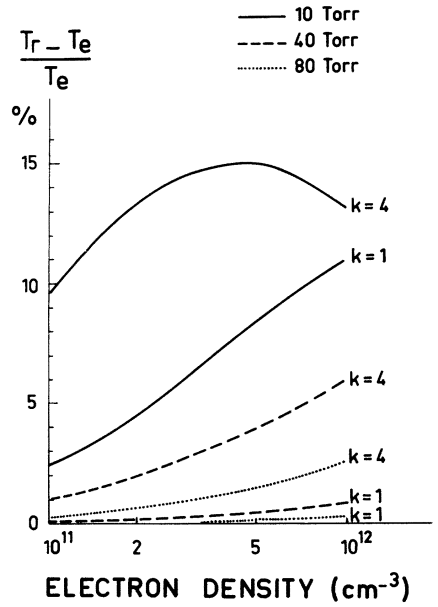

FIG. 9. Effects of the deviation of the energy distribution function on the radiation temperature of an afterglow.

APPENDIX

In a recent article, Johnson and Gerardo[17] suggested that the partition of energy could be approximated by

$$\sum_n (\Delta\epsilon_{ee})_n = \int_{(3/2)kT_e}^{\epsilon_0} \frac{d\epsilon}{1 + (2m/M_{He})(\nu_{e0}/\nu_{ee})} . \quad (21)$$

This was apparently obtained by assuming that both relaxation processes could be assumed to be continuous and writing

$$\frac{d\epsilon}{dt} = -\left(\nu_{ee} + \frac{2m}{M_{He}}\nu_{e0}\right)\epsilon , \quad (22)$$

where $\epsilon >> \frac{3}{2}kT_e$, $\frac{3}{2}kT_0$ and the liberation of energy to the background electrons is

$$\frac{d\epsilon}{dt} = \nu_{ee}\epsilon . \quad (23)$$

Equation (21) can be obtained by taking the ratio of (22) and (23) and integrating. Although the evaluation of this integral was not given, we find the analytical solution for

$$\begin{aligned} &\nu_{ee} = a\epsilon^{-3/2} , \\ &(2m/M_{He})\nu_{e0} = b\epsilon^{1/2} \quad \text{for } \epsilon \leq 3 \text{ eV} \\ &\qquad\qquad = c \qquad \text{for } \epsilon \geq 3 \text{ eV} , \quad (24) \\ &\sum_n (\Delta\epsilon_{ee})_n = [A \arctan(\epsilon/A)]_{(3/2)kT_e}^{3eV} \\ &\qquad + \tfrac{2}{3}k^2\{\tfrac{1}{2}\ln[1 - 3k\sqrt{\epsilon}/(k + \sqrt{\epsilon})^2] \\ &\qquad + \sqrt{3}\arctan(2\sqrt{\epsilon} - k)/k\sqrt{3}\}_{3eV}^{20eV} , \end{aligned}$$

where $A = (a/b)^{1/2}$ and $k = (a/c)^{1/3}$. Comparison between the numerical and analytical solutions we have given show identical results except for energies near $\frac{3}{2}kT_e$.

In discussions about this work, Allis suggested the value of an analytical solution would warrant an additional evaluation of (22). With his aid, we have found

$$\left(\frac{1}{2A}\right)^{3/2}\left(\ln\frac{A - \epsilon^{1/2}(2A)^{1/2} + \epsilon}{A + \epsilon^{1/2}(2A)^{1/2} + \epsilon} - 2\arctan\frac{1}{A\epsilon}\right)_{\epsilon_0}^{\epsilon_1}$$

$$= -b(t_1 - t_0) \quad \text{for } \epsilon \leq 3 \text{ eV} , \quad (25)$$

$$[\ln(a + c\epsilon^{3/2})]_{\epsilon_0}^{\epsilon_1} = -\tfrac{3}{2}c(t_1 - t_0) \qquad \text{for } \epsilon \geq 3 \text{ eV} ,$$

as a solution.

By using this result in the same fashion as the relaxation time in the text, we have found the distribution function to be

$$\begin{aligned} f(\epsilon) &= \frac{1}{4\pi}\left(\frac{m^3}{2}\right)^{1/2}\frac{S}{a + b\epsilon^2} \qquad \text{for } \epsilon \leq 3 \text{ eV} , \\ f(\epsilon) &= \frac{1}{4\pi}\left(\frac{m^3}{2}\right)^{1/2}\frac{S}{a + c\epsilon^{3/2}} \qquad \text{for } \epsilon \geq 3 \text{ eV} , \end{aligned} \quad (26)$$

where

$$\begin{aligned} S &= \gamma N_e M \qquad \text{for } \epsilon > 15 \text{ eV} , \\ S &= \gamma N_e M + \tfrac{1}{2}\beta M^2 \quad \text{for } \epsilon \leq 15 \text{ eV} . \end{aligned}$$

Again the results of the two are identical except

for energies near $\frac{3}{2}kT_e$.

It should be pointed out that although the analytical solutions have been found in these cases, for other applications perhaps more complex, the methods described in the text may be more satisfactory.

[1]R. Deloche, P. Monchicourt, W. E. Wells, and J. Berlande, J. Phys. B (to be published).
[2]P. A. Miller, J. T. Verdeyen, and B. E. Cherrington, Phys. Rev. A **4**, 692 (1971).
[3]C. B. Collins, H. S. Hicks, W. E. Wells, and R. Burton, Phys. Rev. A **6**, 1545 (1972).
[4]J. F. Delpech (private communication).
[5]D. R. Bates and A. E. Kingston, Proc. R. Soc. Lond. **279**, 10 (1964).
[6]J. C. Ingraham and S. C. Brown, Phys. Rev. **138**, 1015 (1965).
[7]J. W. Poukey, J. B. Gerardo, and M. A. Gusinow, Phys. Rev. **179**, 211 (1969); E. R. Mosburg, Phys. Rev. **152**, 166 (1966).
[8]H. Hotop and A. Niehaus, Z. Phys. **228**, 68 (1969).
[9]A. V. Phelps and J. P. Molnar, Phys. Rev. **89**, 1202 (1953).
[10]G. J. Schultz and R. E. Fox, Phys. Rev. **106**, 1179 (1957).
[11]J. L. Delcroix, Report No. III (University of Paris, Orsay) (unpublished).
[12]L. Spitzer, Jr., *Physics of Fully Ionized Gases* (Interscience, New York, 1956).
[13]A. V. Phelps, Phys. Rev. **99**, 1307 (1955).
[14]S. C. Brown, *Basic Data of Plasma Physics* (Wiley, New York, 1959).
[15]J. Berlande, M. Cheret, R. Deloche, A. Gonfalone, and C. Manus, Phys. Rev. A **1**, 887 (1970).
[16]G. Bekefi, *Radiation Processes in Plasmas* (Wiley, New York, 1966).
[17]A. Wayne Johnson and J. B. Gerardo, Phys. Rev. A **5**, 1410 (1972).

PHYSICAL REVIEW A VOLUME 8, NUMBER 1 JULY 1973

Collision Processes Occurring in Decaying Plasmas Produced in Helium-Hydrogen Mixtures*

G. E. Veatch† and H. J. Oskam
Department of Electrical Engineering, University of Minnesota, Minneapolis, Minnesota 55455
(Received 9 October 1972)

The time dependence of the densities of He^+, He_2^+, H^+, H_2^+, H_3^+, HeH^+, and He_2H^+ ions was measured in the afterglow period of plasmas produced in helium containing 0.01, 0.02, and 0.1% hydrogen for total gas pressures varying from 1 to 10 Torr. The rate constant for the ionization of H_2 by $He(2\,^3S)$ was found to be 5.2×10^{-11} cm sec^{-1}. The studies resulted in the observation, for the first time, of the production of H_2^+ by mutual collisions between metastable hydrogen molecules. The radiative lifetime of these molecules was measured to be 2.7 ± 0.2 msec. The occurence of several other collision processes was also established. The mobility of H_3^+ in helium was determined to be $\mu_0 = 40 \pm 0.5$ cm^2 $(V\ sec)^{-1}$.

I. INTRODUCTION

In 1965, Oskam and Mittelstadt[1] published a study of the electron-density decay in helium-hydrogen mixtures after cessation of the discharge pulse. The electron density was measured using the microwave-cavity method. The measurements were performed over a total pressure range 1–32 Torr and a range of hydrogen concentrations 10^{-4}–1%. They measured an effective ambipolar diffusion coefficient D_a, which is defined as

$$(D_a p_0)_{\text{eff}} \equiv p_0 \Lambda^2/\tau_e, \tag{1}$$

where Λ is the characteristic diffusion length of the plasma container related to the fundamental diffusion mode, p_0 is the gas pressure reduced to 0 °C, and τ_e is the measured time constant of the exponential part of the electron-density decay curve.

For gas pressures between 4 and 32 Torr the effective ambipolar diffusion coefficient depended on the discharge-excitation pulse length and varied from $(D_a p_0)_{\text{eff}} = 1350$ to 1650 $cm^2\ sec^{-1}$ Torr. The larger value was obtained for the longest pulse length, which ranged from 0.01 to 5 msec. No satisfactory explanation was found for this behavior.

The only other afterglow studies in helium-hydrogen mixtures of which we are aware were performed by Adams *et al.*[2] using the flowing-afterglow method. They reported rate constants for reactions of He_2^+, HeH^+, HeH_2^+, and He_2H^+ with hydrogen. In order to determine the reasons for the unusual behavior of the effective ambipolar diffusion coefficient observed by Oskam and Mittelstadt, the present mass-spectrometer measurements were performed. In addition, it was believed that information could be obtained about the collision